Drying kinetics and packing of particles of silica-water nanofluid droplets dried in an acoustic levitator

R. Mondragón[1], J. C. Jarque[1], J. E. Juliá[2*], L. Hernández[2]
[1]Instituto de Tecnología Cerámica, Universitat Jaume I, Spain
[2]Departamento de Ingeniería Mecánica y Construcción, Universitat Jaume I, Spain
rosa.mondragon@itc.uji.es, juancarlos.jarque@itc.uji.es, bolivar@emc.uji.es and lhernand@emc.uji.es

Abstract

The spray drying process is used in many industrial applications to produce powders with different characteristics. Drying models based on the reaction engineering approach (REA) have been found promising due to its simplicity and high accuracy at different drying conditions. In this work single droplets of silica-water nanofluids were dried in an acoustic levitator under different experimental conditions of initial solid mass fraction ($0.02 < Y_S < 0.20$), pH value ($2 < pH < 10$), salt concentration ($0\ M < [NaCl] < 0.05\ M$), air temperature ($80ºC < T < 120ºC$), and initial droplet volume ($0.3\ \mu l < V_0 < 0.8\ \mu l$). The drying curves ($X$=f(t)) were experimentally obtained for each test conducted and the REA model was used to model the experimental data. The grains were collected and observed by SEM in order to measure the thickness of the shell formed. Finally, the packing of particles inside the droplet was checked to be constant and equal to the random close packing. This packing can be obtained from the modelling of the viscosity data to the Quemada equation. The final diameter and the packing fraction were used to calculate the shell thickness. Experimental results from the SEM micrographs and theoretical results show a good agreement.

Introduction

In many industrial applications such as ceramics, food products, detergents and pharmaceuticals, the spray drying process is used to produce powders with different characteristics. The main objective of the researchers in this field is to know the effect of the variables that influence the drying process on the final properties to be able to control them and therefore to produce granules of desired characteristics suitable for each application.

Depending on the final application of these grains and their later handling and processing, different micro-structures can be required. That makes of great importance to know the influence of all the variables involved in the drying process on the crust formation, the packing of the particles, the hollowness of the final grain, etc.

The drying behaviour of a liquid-solid suspension droplet can be divided into two stages [1-3]. In the first stage, also known as constant rate period, particles move towards the inner part of the droplet to minimize its surface energy [4, 5]. The surface energy of the liquid-vapor interface is lower than the solid-vapor one so, particles move allowing the droplet surface to be fully wetted and the liquid to evaporate at the droplet surface. As a consequence, the mass transfer rate equals that of an equally sized pure liquid droplet. The diameter, d, decreases following the d^2-relation and the maximum drying rate value is achieved. At the critical moisture content, the entire droplet surface cannot longer be maintained saturated by moisture migration and the second drying period begins. In this period, called falling rate period, a shell is formed at the droplet surface and the evaporation occurs through the pores of the shell. The drying rate continues to decrease as the thickness of the shell increases. If the particles have been able to move or they have had enough time to diffuse inside the droplet before the shell formation, a compact grain will be formed. However, if the particles cannot easily move due to the suspension characteristics or the drying is so fast that there is no time for the particles to diffuse, they will remain in the outer part of the droplet and the external shell will be formed before. As a result, the grains will have a hollow morphology and a higher diameter.

Authors have found the drying models based on reaction engineering approach (REA) promising due to its simplicity and high accuracy at different drying conditions [6-12]. The main theory of the model considers the drying as an activation process in which an energy barrier has to be overcome for moisture removal to occur. In the mathematical expression of the model, the vapor concentration gradient is considered the driving force for the drying. The water removal process is represented by an activation energy which value is zero when the solid is fully covered by water, and increases as the moisture content decreases, due to the difficult of water removal

* Corresponding author: bolivar@emc.uji.es

for low contents. However, the model uses a correlation for the activation energy that depends on the material and drying conditions, and has to be determined experimentally.

Drying models predicting the drying kinetics of single droplets can be used to relate the final powder properties (such as the final grain diameter, mean porosity, compacity, morphology, microstructure, etc.), with the spray dryer design and process parameters. From the drying kinetics the critical moisture content can be determined and the final grain diameter can be calculated [13]. If the packing fraction of the particles inside the shell is known, the degree of hollowness can be predicted.

The packing fraction of the particles in the shell is constant and closer to the maximum packing that particles can achieve, i.e. the random close packing [14, 15]. The maximum packing fraction that the nanoparticles system can achieve (RCP) corresponds to the fluidity limit, ϕ_m. Below this value the nanofluid behaves like a liquid while above the fluidity limit the nanofluid has the properties of a solid. The graphical representation of viscosity versus the volume fraction allows obtaining the fluidity limit, concentration at which the viscosity takes infinite value. Krieger and Dougherty, and Quemada [16, 17] proposed equations to model the viscosity of numerous suspensions with particles different in nature, that allows the knowledge of the fluidity limit, and hence the random close packing, for each particulate system.

In this work single droplets of silica-water nanofluids were dried in an acoustic levitator under different experimental conditions of initial solid mass fraction, Y_S, *pH* value, salt concentration, *[NaCl]*, air temperature, T, and initial droplet volume, V_0. The drying curves (X=f(t)) were experimentally obtained for each test conducted and the REA model was used to model the experimental data. The fluidity limit and the maximum packing fraction were obtained for this system using the Quemada equation to model the viscosity data. The packing fraction and the final diameter were used to calculate the shell thickness. The dried grains were collected to observe the internal microstructure by means of scattering electron microscopy and the shell thickness was measured and compared to that previously calculated.

Materials and Experimental Methods

All the experiments performed in this study were carried out with silica-water nanofluids. Commercial fumed silica (Aerosil 200 with primary units of 12 nm) provided by Degussa was purchased in dry powder. The isoelectric point (IEP) was established at *pH* = 2 from the measurement of the zeta potential at different *pH* values using a Zetasizer Nano ZS (Malvern Instruments). Nanofluids with different particle concentrations were prepared by adding distilled water containing different concentration of NaCl salt to the defined amounts of nanoparticles. The dispersion was performed using an ultrasonic probe (UP400s from Hielscher Company). Initially, the mixture of nanoparticles with the water or salt solution is submitted to a 3-minute sonication treatment. After this, the *pH* of the nanofluid is modified adding HCl or NaOH solutions. Finally, to ensure a correct dispersion of all the components, the nanofluids are submitted to a second sonication treatment during 2 minutes.

The viscosity of the nanofluids was obtained at 25ºC by conducting tests under steady state conditions using a Bohlin CVO-120 rheometer (Malvern Instruments Ltd., UK). A double gap (DG 40/50) device composed of two concentric cylinders suitable for low viscosity suspensions was used. Before each test, a pre-treatment, in which the samples are submitted to a constant shear stress, was applied to the nanofluids for 30 seconds to ensure similar starting conditions for all of them.

Single droplets were dried in an ultrasonic levitator modified in order to work at high temperature conditions. The experimental set-up was described elsewhere [18]. The entire system is composed of an ultrasonic levitator in which the chamber that contains the droplet is heated by electric heaters. This chamber is isolated from the one that contains the piezoelectric transducer which is cooled by forced convection to ensure temperatures lower than 60 ºC and avoid damages in the transducer. An optical system consisting of a CMOS camera and back-light illumination system are used to record and measure the droplet cross-sectional area and vertical position of the droplet during the drying process. Finally, a gas conditioning system is used to control the temperature, flow rate and relative humidity of the air inside the levitator tube.

The images of the drying process recorded with the camera were processed with Matlab. Thus, the equivalent diameter and position of the droplet during all the drying stages were obtained.

The instantaneous mass transfer rate for the first drying period ($m_{L,1}$) was calculated from the decrease of the droplet diameter. This mass transfer rate is defined as,

$$m_{L,1} = -\frac{\pi}{6}\rho_L \frac{d_1^3 - d_2^3}{t_1 - t_2} \tag{1}$$

where ρ_L is the liquid density and the sub-indexes 1 and 2 denote two consecutive instants during the drying process.

The mass transfer rate of the second drying period ($m_{L,2}$) is calculated using the position of the droplet inside the acoustic field. If this position is assumed to be dependent on the droplet density, the mass transfer rate during this period can be calculated as,

$$m_{L,2} = \frac{M_{21}}{t - t_{21}} \frac{y(t) - y_{21}}{y_{22} - y_{21}} \tag{2}$$

where y_{21} and y_{22} are the droplet positions at the beginning and the end of the second drying period respectively, $y(t)$ is the instantaneous position of the droplet, and M_{21} is the liquid mass content in the droplet at the end of the first drying period previous to the shell formation.

With the initial water content and the liquid evaporation rates, the quantity of water present in the droplet/grain at each moment, can be easily calculated. The dry basis moisture, X, is defined as the ratio between the water and solid contents:

$$X = \frac{M_L(t)}{M_S} \tag{3}$$

where M_L is the mass of water and M_S is the mass of solid present in the droplet, which remains constant during all the drying process.

Finally, the internal microstructure of the grains obtained was observed by means of Scattering Electron Microscopy using a FEI Quanta 200F microscope. The grains were cut and coated with platinum in order to obtain cross sections and to observe the internal shell formed during the drying process, to measure it. Images of the shell and the arrangement of the nanoparticles in it were taken.

Results and Discussion

Drying tests were carried out under different experimental conditions: initial solid mass fraction ($0.02 < Y_S < 0.20$), pH value ($2 < pH < 10$), salt concentration ($0\ \text{M} < [NaCl] < 0.05\ \text{M}$), air temperature ($80ºC < T < 120ºC$), and initial droplet volume ($0.3\ \mu l < V_0 < 0.8\ \mu l$). For each of the measured experiments, the evolution of the squared-diameter and the position of the droplet were obtained.

For the first drying period and intervals of diameter variation, Equation 1 was used to obtain the mass transfer rate. For the second drying period and intervals of constant diameter, the mass transfer rate was obtained from the evolution of position by means of Equation 2. With the initial moisture content and the water evaporation along the process, the droplet/grain moisture content was obtained by means of Equation 3.

Drying curves were modeled using the REA model (Reaction Engineering Approach):

$$\frac{dX}{dt} = -\frac{h_m A}{M_S}\left[\rho_{v,sat} \exp\left(-\frac{\Delta E_V}{R\, T_d}\right) - \rho_{v,a}\right] \tag{4}$$

where X is the dry basis moisture content, h_m is the mass transfer coefficient, A is the droplet area, R is the gas constant, T_d is the droplet temperature, $\rho_{v,a}$ is the vapor density in the drying air, $\rho_{v,sat}$ is the saturation vapor concentration (evaluated at the droplet temperature, T_d) and ΔE_v is the activation energy for the drying process to take place, which depends on the material and the drying conditions.

The mass transfer coefficients were previously obtained experimentally from the evolution of the diameter of pure water droplets under the experimental conditions tested in this work. The values obtained were used to model the drying curves of the nanofluids.

Figure 1 shows the experimental data and the theoretical curves obtained by means of REA model.

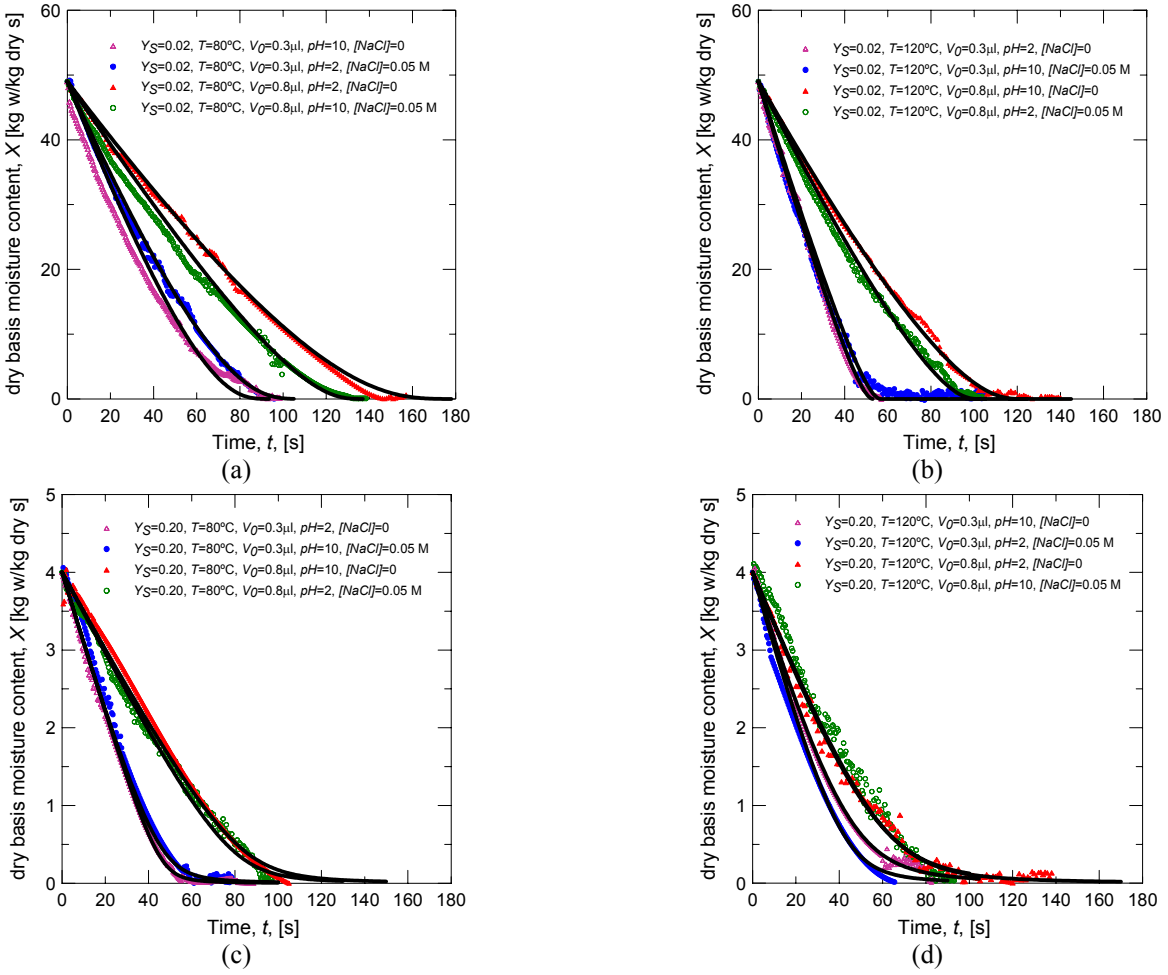

Figure 1 Drying curves: experimental data and REA model. (a) Ys=0.02, T=80ºC, (b) Ys=0.02, T=120ºC, (c) Ys=0.20, T=80ºC, (d) Ys=0.20, T=120ºC.

The dried grains were collected and observed by Scattering Electron Microscopy. Figure 2 shows grains obtained from the drying of droplets under different experimental conditions. The shell thickness for all grains collected in each experiment was measured.

The shell thickness, s, can be theoretically calculated with the Equation 5. However, the packing fraction of the particles inside is needed.

$$s = r_G - \left(r_G^3 - \frac{r_{0,d}^3 \cdot Y_S \cdot \rho_{0,d} / \rho_S}{\phi_{Shell}} \right)^{1/3} \tag{5}$$

where r_G is the grain radius, $r_{0,d}$ is the initial droplet radius, $\rho_{0,d}$ is the initial density of the droplet, Y_S is the solid mass fraction and ϕ_{Shell} is the packing fraction.

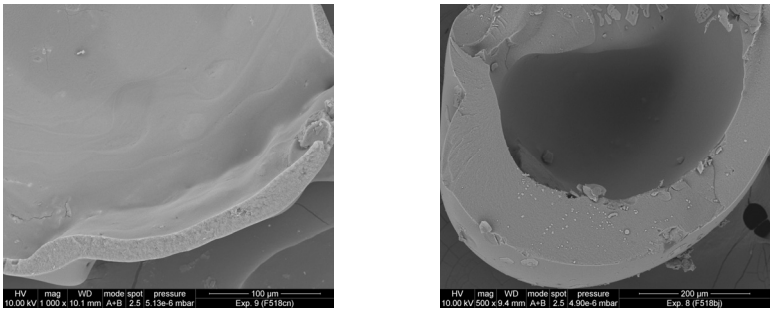

(a) **(b)**

Figure 2 Grains dried at different drying conditions: (a) Y_S =0.02, *pH* =2, *[NaCl]*=0, *T*=120°C, V_0=0.3 µl, (b) Y_S =0.20, *pH* =10, *[NaCl]*=0.05 M, *T*=80°C, V_0=0.3 µl.

.

In order to calculate the fluidity limits and the maximum packing fraction of the particles, Quemada equation was used to model the viscosity data at different solid contents for the two *pH* values studied (2 and 10).

$$\eta_r = \frac{\eta}{\eta_F} = \left(1 - \frac{\phi}{\phi_m}\right)^{-2} \tag{6}$$

where η_r is the relative viscosity, η, is the viscosity of the nanofluid, η_F is the viscosity of the base fluid and ϕ_m is the fluidity limit.

Nanofluids where prepared at volume fractions ranging from 0.002 to 0.132, which corresponds to mass fractions from 0.005 to 0.25. These solid contents cover a wide range of viscosities and that makes possible the fitting of the data to the equation. To model the evolution of the viscosity results with the solid content, effective volume fractions are needed [19].

$$\phi_{eff} = \phi \left(\frac{r_p + \kappa^{-1}}{r_p}\right)^3 \tag{7}$$

where r_p is the radius of the primary particles and κ^{-1} is the thickness of the electrical double layer which can be calculated from the ionic strength of the medium, *I:*

$$\kappa^{-1} = 0.215 \cdot 10^{-9} \cdot \sqrt{I} \tag{8}$$

In Figure 3 experimental data are represented together with the theoretical curves corresponding to the Quemada equation. It can be seen that the viscosity results are in good agreement with the model.

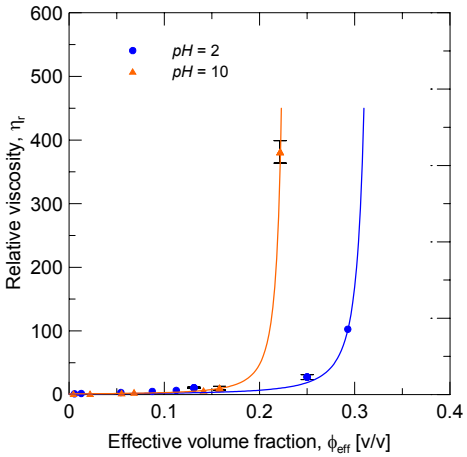

Figure 3 Evolution of relative viscosity with effective volume fraction and *pH*. Experimental data and modelled curve.

As can be seen, at *pH*=2 (IEP) the maximum value for the fluidity limit is achieved (ϕ_m = 0.33), which represents the Random Close Packing and equals the packing fraction of the particles inside the shell formed. In this case Van der Waals cohesive forces are predominant. These forces restrict the relative movement of particles resulting in agglomerates with presence of large pores and worst packings than in the case of hard spheres. When the *pH* value is increased, particles get negative charge and an electrical layer is formed around them. The repulsion generated between particles leads them to remain apart from each other resulting in higher viscosities (secondary electroviscous effect) and less compact packings.

Results obtained from Equation 5 for the shell thickness were plotted versus the ones measured from the micrographs. Figure 4 shows the fitting of the data in which a very good agreement between theoretical and experimental results can be observed.

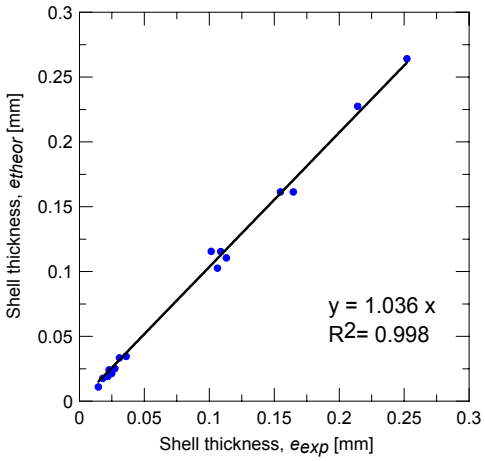

Figure 4 Shell thickness determined experimentally and theoretically.

Therefore, the packing of the particles in the shell can be said to be constant and equal to the maximum packing that particles can achieve: random close packing. The packing fraction in independent on the solid content, the drying temperature, the *pH* of the suspension, the salt content and the initial droplet volume.

Summary and Conclusions

Single droplets of silica-water nanofluids were dried under different experimental conditions of solid content, *pH* value, salt concentration, drying temperature and droplet volume. Experimental drying curves were modeled using the REA model. Theoretical curves showed a good agreement with the experimental data.

All the grains collected were observed by means of SEM and the shell thickness was measured. In order to calculate the theoretical thickness, the packing fraction was needed. This packing of particles inside the droplet was checked to be constant for a particular system and equal to the random close packing. Its value can be obtained from the modelling of the viscosity data to the Quemada equation. For nanoparticles the value of the packing fraction is lower than for hard microparticles due to the presence of cohesive forces that difficult the movement and rearrangement of particles.

Finally, experimental and theoretical results for the shell thickness were compared and the results showed a good agreement.

As a conclusion, from the drying curves, knowing the packing of the particles in the shell, the final grain diameter and the shell thickness can be obtained in order to evaluate the degree of hollowness of the grains produced.

Acknowledgements

R. Mondragón thanks the Spanish Ministry of Education for a pre-doctoral fellowship (FPU program, Ref. AP2008-01077).

The authors gratefully acknowledge the financial support from Fundació Caixa Castelló-Bancaixa (project: P11B2009-27) and the Spanish Ministry of Science and Innovation (project: CTQ2010-21321-C02-01).

References

[1] Masters, K., *Spray drying handbook,* Longman Scientific and Technical, 1991.
[2] Kastner, O., Brenn, G., Rensink, D., Tropea, C., *Chemical Engineering and Technology* 24: 335-339 (2001).
[3] Mezhericher, M., Levy, A., Borde, I., *Drying Technology* 28: 278-293 (2010).
[4] Hadinoto, K., Phanapavudhikul, P., Kewu, Z., Tan, R.B.H., *Industrial and Engineering Chemistry Research* 45: 3697-3706 (2006).
[5] Hadinoto, K., Cheow, W.S., *Drug Development and Industrial Pharmacy* 35: 1169-1179 (2009).
[6] Chen, X.D., *Drying Technology* 26: 627-639 (2008).
[7] Chen, X.D., Lin, S.X.Q., *AIChE Journal* 51: 1790-1799 (2005).
[8] Chen, X.D., Xie, G.Z., *Food and Bioproduct Processes* 75: 213-222 (1997).
[9] Fu, N., Woo, M.W., Lin, S.X.Q., Zhou, Z., Chen, X.D., *Chemical Engineering Science* 66: 1738-1747 (2011).
[10] Lin, S.X.Q., Chen, X.D., *Drying Technology* 24: 1329-1334 (2006).
[11] Patel, K.C., Chen, X.D., *Journal of Food Process Engineering* 28: 567-594 (2005).
[12] Woo, M.W., Wan Daud, W.R., Mujumdar, A.S., Meor Talib, M.Z., Hua, W.Z., Tasirin, S.M., *Chemical Engineering Research and Design* 86: 1038-1048 (2008).
[13] Mezhericher, M., Levy, A., Borde, I., *Drying Technology* 25: 1035-1042 (2007).
[14] Sen, D., Khan, A., Bahadur, J., Mazumder, S., Sapra, B.K., *Journal of Colloid and Interface Science* 347: 25-30 (2010).
[15] Bahadur, J., Sen, D., Mazumder, S., Paul, B., Khan, A., Ghosh, G., *Journal of Colloid and Interface Science* 351: 357-364 (2010).
[16] Krieger, I.M., Dougherty, T.J., *Transactions of the Society of Rheology* 3: 137–152 (1959).
[17] Quemada, D., *Rheological Acta* 16: 82-94 (1977).
[18] Mondragon, R., Hernandez, L., Julia, J.E., Jarque, J.C., Chiva, S., Zaitone, B., Tropea, C., *Chemical Engineering Science* 66: 2734-2744 (2011).
[19] Quemada, D., *European Physical Journal of Applied Physics* 1: 119-127 (1998).